A dynamical correlated effective-field treatment of the magnetic excitations in the singlet ground state antiferromagnet $RbFeBr_3$

1992 J. Phys.: Condens. Matter 4 6977

(http://iopscience.iop.org/0953-8984/4/33/011)

J. Phys.: Condens. Matter 4 (1992) 6977–6992. Printed in the UK

A dynamical correlated effective-field treatment of the magnetic excitations in the singlet ground state antiferromagnet $RbFeBr_3$

A Harrison and D Visser†

Oxford University, Inorganic Chemistry Laboratory, South Parks Road, Oxford OX1 3QR, UK

Received 6 March 1992, in final form 22 May 1992

Abstract. The dispersion of magnetic excitations in the pseudo-one-dimensional induced-moment antiferromagnet $RbFeBr_3$ has been measured at 4.5 K using inelastic neutron scattering. Below $T_N = 5.5$ K a distinct dispersion of magnetic excitations was observed along and between the magnetic chains. The energies and scattering intensities of these excitations was described well using Suzuki's DCEFA model. The components of intrachain superexchange perpendicular and parallel to the crystal c-axis were found to be $J_1^{\perp} = -0.40(1)$ and $J_1^{\parallel} = -0.43(4)$ meV respectively. The corresponding interchain exchange constants were found to be $J_2^{\perp} = -0.044(3)$ and $J_2^{\parallel} = -0.065(13)$ meV. Above T_N the magnetic excitations at $(001)_N$ dropped in intensity and their small renormalization in energy was described well by the DCEFA model.

1. Introduction

$RbFeBr_3$ is one of a series of isomorphous $AFeX_3$ compounds (A=Rb, Cs, Tl or NH_4 and X=Cl or Br) that have been used as model magnets (Achiwa 1969, Yoshizawa *et al* 1980, Steiner *et al* 1981, Wada *et al* 1982, Shiba and Suzuki 1982, Lindgård 1983, Knop *et al* 1983, Suzuki 1983a, c, Visser and Steigenberger 1984, Harrison 1986, Visser and Harrison 1988, Dorner *et al* 1988, Harrison and Visser 1989a, b, Harrison *et al* 1991, Plumer and Caillé 1991). The magnetic behaviour of these materials is the result of a delicate balance between several competing interactions. All the salts listed above crystallize in the hexagonal perovskite structure, but have the following differences in magnetic properties.

(i) The chlorides behave as pseudo one-dimensional ferromagnets, whereas the bromides that have been characterized so far (A = Rb, Cs, NH_4) (Visser and Harrison 1988, Harrison *et al* 1991) are pseudo one-dimensional antiferromagnets.

(ii) The caesium salts behave as singlet ground state materials, but the rubidium, ammonium and thallium salts that have been studied have magnetic ground states with long-range magnetic order at low temperatures.

† Present address: Loughborough University of Technology, Department of Physics, Loughborough LE11 3TU, UK.

0953-8984/92/336977+16$04.50

The task of explaining the relationship between magnetic character and the chemical composition or changes in the superexchange bridging angles depends on reliable values of exchange parameters and ligand field parameters. Previous measurements on $AFeX_3$ magnets have yielded a wide distribution of values for these quantities and it is clear from table 1 that they depend very much on the experimental method and the model used to interpret the data. In this paper we seek to provide a reliable set of magnetic parameters for $RbFeBr_3$ using a technique that probes the magnetic susceptibility over both energy and wavevector, namely inelastic neutron scattering. We interpret the data using a model appropriate to this class of material and compare our results with those for other $AFeX_3$ magnets.

1.1. Properties of $RbFeBr_3$ and related materials

1.1.1. The crystal structure of $RbFeBr_3$. At room temperature the space group of $RbFeBr_3$ is $P6_3/mmc$. Chains of face-sharing $FeBr_6^{4-}$ octahedra lie parallel to the c-axis, separated by Rb^+ ions. At 108 K a structural phase transition occurs (Harrison and Visser 1989a) in which two-thirds of the Fe chains (A sites) move out of the basal plane by about 0.5 Å to form a honeycomb lattice, leaving the remaining chains (B sites) arranged on a triangular lattice. The unit cell expands in volume by a factor of 3 ($a' = \sqrt{3}a, c' = c$) and the new space group is $P6_3cm$, the structure being the same as that of $KNiCl_3$ at room temperature (Visser and Prodan 1980). The distortion does not alter the environment of the iron atoms sufficiently to allow the A and B sites to be distinguished by Mössbauer spectroscopy.

1.1.2. Electronic and magnetic properties. In the weak-field coupling scheme the cubic component of the ligand field acts on the free-ion ground term ^5D of Fe^{2+} to produce a lower orbital triplet ($^5T_2$) and an orbital doublet (^5E) at an energy of 6,500 cm^{-1} (Putnik *et al* 1976). The $^5T_2$ term is split further by spin–orbit coupling, λ', and by the trigonal component of the ligand field, Δ'. The Hamiltonian representing these perturbations may be written as

$$H_i = \Delta'(L_{iz}'^2 - 2/3) + \lambda' \boldsymbol{L}'_i \cdot \boldsymbol{S}'_i \tag{1}$$

where $S' = 2$ and, using the isomorphism of the symmetry groups representing T_2 and P terms, $L = 1$. $\lambda' = -k\lambda$, where k is the orbital reduction factor. Among the 15 eigenstates we find a singlet ground state, $|m_J = 0\rangle$, and an excited doublet, $|m_J = \pm 1\rangle$, at an energy of about 10 cm^{-1}. The next-nearest excited state lies at about 150 cm^{-1}. Consequently, at low temperatures we may describe the electronic and magnetic properties of $RbFeBr_3$ well using the effective spin Hamiltonian

$$H_i = DS_{iz}^2 - \sum_j 2[J_1^{\perp}(S_{ix}S_{jx} + S_{iy}S_{jy}) + J_1^{\parallel}S_{iz}S_{jz}] - \sum_{j'} 2[J_2^{\perp}(S_{ix}S_{j'x} + S_{iy}S_{j'y}) + J_2^{\parallel}S_{iz}S_{j'z}] \tag{2}$$

where the sums are over the nearest neighbours j in the chains and j' between chains. J_1^{γ} and J_2^{γ} are the intra- and interchain exchange constants ($\gamma = \perp, \parallel$) and D is the single-ion anisotropy. Clearly, D, J_1^{γ} and J_2^{γ} all depend on Δ'/λ'. If D/J_K (where J_K is the optimum exchange energy and corresponds to a magnetic ordering

Table 1. Electronic and magnetic parameters for $AFeX_3$ compounds. All energies are in meV, and the numbers in brackets give the source of the data, listed below the table. Dq is the cubic component of the ligand field, B and C are the Racah parameters, λ is the spin-orbit coupling constant, Δ the trigonal component of the ligand field and D the single-ion anisotropy that results from Δ in the $S = 1$ single-ion Hamiltonian. k is the orbital reduction factor and J_1^γ and J_2^γ denote the components of the intra- and interchain superexchange constants ($\gamma = \perp$, $\|$, defined relative to the crystal c-axis).

Parameter	Compound			
	$RbFeCl_3$	$RbFeBr_3$	$CsFeCl_3$	$CsFeBr_3$
Dq	90.62[3]	81.25[3]	90.62[3]	81.25[3]
B	109.4	112.5[3]	109.4[3]	112.5[3]
C	475[3]	450[3]	475[3]	450[3]
λ	9.185[1] 12.88(8)	10[4]	9.82[2]	
Δ	7.59(1)	13[4]	8.64[2]	
D	1.525[3] 1.0[5] 0.7[6C] 2.45[6E] 1.71[6S] 2.08[8] 1.92[12]	1–1.1[4]	1.625[2] 1.23[6C] 2.18[6E] 1.01[10] 2.1[11] 2.03[13]	1.85 [14] 2.48 [15]
k	0.85[4]	0.78[4]		
$J_1^{\|}$	0.625[1] 0.25[5] 0.375[6C] 0.075[6E] 0.4625[6S] 0.125[8] 0.52[12]	−0.883[4]	0.313[2] 0.0002[6E] 0.616[7] 0.4[10] 0.262[11] 0.25[13]	−0.42 [14] −0.264 [15]
$J_1^{\perp}$	1.375[1] 0.338[5] 0.525[6C] 0.275[6E] 0.488[6S] 0.275[8] 0.405[12]	−0.525[4]	0.625[2] 0.325[6C] 0.227[6E]	−0.38 [14]
J_2	−0.048[6C] −0.025[6E] −0.068[6S] −0.034[12]	−0.025[4] −0.0833[9]	−0.012[6C] −0.012[6E] −0.009[7] −0.017[11] −0.017[13]	−0.039 [14] −0.0248 [15]

[1] Montano *et al* (1973). Mössbauer + pair model. [2] Montano *et al* (1974). Mössbauer + pair model. [3] Putnik *et al* (1976). Optical absorption. [4] Lines and Eibschutz (1975). Magnetic susceptibility and correlated effective-field (CEF) model. [5] Eibschutz *et al* (1975). Magnetic susceptibility and CEF model. [6] Yoshizawa *et al* (1980). Inelastic neutron scattering with CEF (C), exciton (E) and spin-wave (S) models for magnon dispersion. [7] Steiner *et al* (1981). Inelastic neutron scattering with heuristic expression. [8] Suzuki (1981). Magnetic susceptibility, inelastic neutron scattering and far-infrared data with DCEFA model. [9] Adachi *et al* (1983). Heat capacity data with molecular-field approximation (MFA). [10] Baines *et al* (1983). Mössbauer data with MFA. [11] Lindgård (1983). Inelastic neutron scattering with correlation model. [12] Suzuki (1983c). Inelastic neutron scattering with DCEFA model. [13] Knop and Steiner (1984). Inelastic neutron scattering with correlation model. [14] Visser and Harrison (1988) Inelastic neutron scattering with DCEFA model. [15] Schmid *et al* (1992b) Inelastic neutron scattering with correlation model.

vector K) lies above a critical value, the ground state acquires a finite magnetic moment: three-dimensional magnetic long-range order occurs in the rubidium and thallium salts at low temperatures, but the caesium salts, in which the cell constants are larger and the exchange constants smaller, behave as 'true' singlet ground state materials. Néel temperatures, where applicable, are given in table 1. However, if a magnetic field is applied parallel to the crystal c-axis, the excited doublet is Zeeman-split and mixed into the ground state. In this way magnetic long-range order may be induced in $CsFeCl_3$ (Haseda *et al* 1981, Steiner *et al* 1981, Dickson 1981, Dorner *et al* 1990, Knop *et al* 1983, Chiba *et al* 1988) and $CsFeBr_3$ (Visser and Steigenberger 1984, Visser *et al* 1991a, Schmid *et al* 1992a, b).

The interchain exchange J_2 propagates through two bromine atoms in the bridge Fe–Br–Br–Fe. Direct Fe–Fe orbital overlap is negligible here, so magnetic exchange is almost entirely due to superexchange involving valence p orbitals on bromine and the orbitally non-degenerate orbitals of e symmetry on the iron atoms. Consequently, J_2 should have a Heisenberg symmetry and should be negative in sign, since the Fe–Br–Br angle of 134° lies well above the value beyond which the antiferromagnetic 'kinetic' component of exchange dominates the ferromagnetic 'potential' component.

There is much less certainty about the sign of J_1. The Fe–Br–Fe bridging angle lies in the transition region where ferromagnetic 'potential' terms give way to antiferromagnetic 'kinetic' terms as the angle is lowered (for empirical illustrations of this see Hatfield *et al* 1983). Indeed, the chloride has ferromagnetic J_1 and the bromide, with a smaller value of bridging angle θ and a more covalent superexchange bridge, has antiferromagnetic J_1.

In addition to the path involving orbital overlap between the e symmetry d orbitals on iron and the p orbitals on bromine, there may be a significant direct component of exchange across the shared face of the $FeBr_6^{4-}$ trigonally distorted octahedra (Goodenough 1960). This would involve the orbitally degenerate t_2-symmetry d orbitals and give a non-Heisenberg component to the exchange parameters. Lines and Eibschutz (1975) and Eibschutz *et al* (1975) considered this to be significant and antiferromagnetic for the chloride, but insignificant for the bromide in which the Fe–Fe separation is much larger. Goodenough (1960) considered such exchange to be ferromagnetic and weak for the case of an interaction between two cations with greater than half-filled d subshells.

Finally, the inequivalence of the A and B iron sites in the low-temperature structural phase of $RbFeBr_3$ may lead to an inequivalence in the magnetic exchange between these sites. The shorter A–A distance is expected to lead to an increased intersite magnetic exchange constant J_2 (A–A) relative to the A–B site exchange J_2(A–B). The heat capacity measurements of Adachi *et al* (1983) revealed two transitions at low temperatures: there was a sharp anomaly at 5.61 ± 0.02 K, and a broad weak one at 2.00 ± 0.04 K. The first transition was interpreted as being from a paramagnetic to a 'disordered' phase in which the moments on the A sites freeze in a bipartite antiferromagnetic array, leaving the B sites disordered. At lower temperatures the B-site moments contribute to the magnetic long-range order,forming a 120° array with the A sites. Suzuki and Shirai (1986) calculated magnon dispersion curves for $RbFeBr_3$ using the molecular field approximation. As the ratio of J_2(A–A)/J_2(A–B) was changed from unity, the degeneracies of the magnon energies at the Brillouin zone centre was removed. However, for reasonable values of J_2(A–A)/J_2(A–B) the splitting of the dispersion curves is expected to be very small. Even when this ratio took the unrealistically high value of 1.25 the splittings were about 0.3 D, which is

0.3–0.5 meV if we substitute previous estimates of D. More recently (Visser 1990) the sublattice magnetization of $RbFeBr_3$ has been measured by neutron scattering down to 1.3 K. The curve has an anomaly at 2.0 K which is consistent with a transition from the partially disordered to the six-sublattice magnetic phase.

1.2. INS characterization of $RbFeBr_3$

In a previous communication (Harrison and Visser 1989a) we reported an inelastic neutron scattering study of the dispersion of magnetic excitations in $RbFeBr_3$ at 4.5 K. We found that the form of the dispersion parallel to the crystal c-axis is unique among insulating ordered antiferromagnets: the periodicity of the dispersion in this direction was *half* that expected for a one-dimensional antiferromagnet. The energy of these excitations rose continuously from $l = 1$ to $l = 2$ rather than passing through a maximum at $l = 1.5$ and falling to another minimum at $l = 2$ (where l is defined relative to the magnetic unit cell).

Loveluck and Lovesey (1975) considered the effect of increasing the ratio D/J_1 on the magnon dispersion in an easy-plane one-dimensional magnet with Heisenberg exchange. The gap at $l = 2.0$ for the branch corresponding to in-plane (xy) fluctuations was shown to increase, and the maximum in the dispersion moved from $l = 1.5$ to $l = 2.0$, remaining at that value for $D/J_1 > 2$. This model was found to describe the form of the dispersion well, but strictly speaking it is invalid for an induced-moment system, and the values of D and J_1 derived using it are physically unreasonable. We also obtained a good fit to the data using an excitonic model with the molecular field approximation (MFA). Again, the values of D and J_1 derived with this model are suspect because the MFA neglects local fluctuations in the magnetic exchange field, which are important for induced-moment low-dimensional magnets.

In this paper we present a description of the magnetic excitations in $RbFeBr_3$ in the intermediate magnetically ordered phase as well as new data taken in the paramagnetic phase at temperatures up to 30 K. We interpret our data with the aid of a model that *does* describe local fluctuations in the exchange field—the dynamical correlated effective-field approximation (DCEFA) (Suzuki 1983b).

2. Theories of magnetic excitations in singlet ground state magnets

The use of spin-wave theory in describing the dispersion of magnetic excitations in induced-moment magnets such as $AFeX_3$ violates one of the conditions of spin-wave theory, namely that the excitations are not small deviations from a known ordered ground state. The failings of spin-wave models in describing the magnetic excitations in $RbFeBr_3$ have been discussed by Harrison and Visser (1989a). For such a material, excitonic models are to be preferred. In order to derive an expression for the generalized susceptibility, $\chi^{\alpha\beta}(q, \omega)$, it is necessary to decouple products of operators such as $S_i S_j$, converting them to sums of expressions in just one spin operator. This is most easily done using the MFA, which involves the substitution

$$S_{i\gamma} S_{j\gamma} \rightarrow S_{i\gamma}\langle S_{j\gamma}\rangle + S_{j\gamma}\langle S_{i\gamma}\rangle \tag{3}$$

where $\gamma = x, y, z$. $\langle S_{i\gamma}\rangle$ is the expectation value of the operator $S_{i\gamma}$, and may be calculated self-consistently from the thermal average of $S_{i\gamma}$ over the single-ion

crystal field levels, or from $\chi^{\alpha\beta}(q, \omega)$ with the aid of the random phase approximation (RPA). The RPA method may be modified by introducing the effect of nearest-neighbour spin correlations (Callen 1963), which may cause the local exchange field to deviate substantially from the ensemble average. This 'correlated effective-field approximation' (Lines 1974) involves the substitution

$$S_{i\gamma}S_{j\gamma} \rightarrow S_{i\gamma}[\langle S_{j\gamma}\rangle + \alpha(S_{i\gamma} - \langle S_{i\gamma}\rangle)] + S_{j\gamma}[\langle S_{j\gamma}\rangle + \alpha(S_{j\gamma} - \langle S_{j\gamma}\rangle)] \tag{4}$$

where α is a parameter that describes the nearest-neighbour magnetic correlations. Suzuki *et al* (1977) showed that Lines' model had certain non-physical consequences which could be corrected by taking an isotropic correlation parameter α which was derived self-consistently using a fluctuation-dissipation expression involving the dynamic susceptibility $\chi^{+-}(q, \omega)$. This approach was called the dynamical CEF approximation (DCEFA).

Lindgård (1984a) pointed out that both the RPA and the CEF approaches ignore magnon–magnon interactions. By including coupling between excitations their lifetimes become finite and their energies may be significantly altered. The effects of magnon–magnon coupling are seen most strongly for magnets at temperatures above T_N or for magnets with pronounced induced-moment character. However, Suzuki's model is presented in the literature in a very general form applicable to any singlet–doublet system. An explicit expression is given for $\chi^{\alpha\beta}(q, \omega)$ which may be readily solved by numerical methods such as that described by Buyers *et al* (1975). Furthermore, Suzuki has performed a thorough study of the magnetic properties of $RbFeCl_3$ above and below T_N and derived a consistent set of exchange parameters to explain the behaviour in both temperature regimes (Suzuki 1983a, c). Thus we shall use Suzuki's model to obtain a consistent set of magnetic parameters $RbFeBr_3$ and $RbFeCl_3$. The extension of Suzuki's model to the paramagnetic phase for this specific case is described in the appendix.

3. Experiment

The sample of $RbFeBr_3$ used in all the experiments was grown by Dr P J Walker of the Clarendon Laboratory, Oxford, by the Bridgman method. It was cylindrical in shape, measuring 15 mm long by 10 mm in diameter and mounted with the $(0\ 0\ 1)_N$ and $(1\ 1\ 0)_N$ reflections in the horizontal scattering plane.

Inelastic neutron scattering experiments were performed on this sample using the Pluto Triple Axis Spectrometer (TAS), AERE, Harwell. Two experimental setups were used, according to the type of measurement. First, a relatively high flux at a wavelength of 2.3512 Å was provided using the (0 0 2) reflection of pyrolytic graphite. The dispersion of the magnetic excitations was then measured by the constant-Q method along $[00l]_N$ and $[\frac{1}{3}\frac{1}{3}l]_N$ ($l = 1 \rightarrow 2$) and along $[hk1]_N$ and $[hk2]_N$ ($h = k = 0 \rightarrow 1$) at 4.5 K. The temperature dependence of these excitations was also studied up to 30 K. The low scattering intensity of the excitations at high values of $|Q|$ and high temperatures limited such measurements to points near $(\frac{1}{3}\frac{1}{3}1)_N$ and $(0\ 0\ 1)_N$. The positions of the experimental measurements in reciprocal space are indicated in figure 1.

The second set of measurements used the (1 1 1) reflection from an aluminium monochromator to provide higher resolution at a wavelength of $\lambda = 2.391$ Å. In

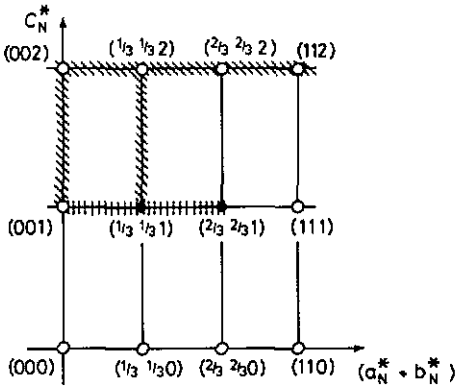

Figure 1. A reciprocal space diagram for $RbFeBr_3$ showing the scattering plane in the present experiment. The axes lie along c_N and $(a_N + b_N)$. Magnetic Bragg points are denoted by ● and nuclear Bragg peaks by ○. The regions scanned with the spectrometer are hatched diagonally for measurements with the pyrolytic graphite monochromator and vertically for measurements with the aluminium monochromator.

both cases the pyrolytic graphite (0 0 2) reflection was used as the analyser and the collimation was provided by soller slits of 20′ (M–S), 30′ (S–A) and 40′ (A–D) (where M, S, A and D are monochromator, sample, analyser and detector). The incoherent elastic neutron scattering at the magnetic reflection $(\frac{1}{3}\frac{1}{3}1)_N$ had widths in energy of 0.6 meV and 0.3 meV with the pyrolitic graphite and aluminium monochromators respectively. Thus, a more careful study of the dispersion along $[hk1]_N$ $(h = k = 0 \rightarrow 1)$ was performed with the second experimental arrangement. Study of the dispersion of the magnetic excitations at higher Q was limited by the lower neutron flux provided by the aluminium monochromator. In both experimental arrangements contamination of the incident beam by neutrons of wavelength $\lambda/2$ was reduced using a pyrolytic graphite plate as a filter.

4. Results

The inelastic neutron scattering measurements at 4.5 K showed distinct dispersion of magnetic excitations along and between the magnetic chains. The scattering intensity fell off rapidly as the temperature was raised, but dispersion along the chain axis persisted well above T_N, showing a small degree of renormalization.

The inelastic neutron scattering peaks were least-squares-fitted to Lorentzian curves convoluted with the Gaussian instrumental resolution function. Examples of fits to the data are presented in figure 2. The width of the Gaussian peak was calculated with the program RESCAL at AERE, Harwell for which the input data were provided by a set of careful measurements in energy and reciprocal space of several Bragg peaks. The results of the peak fitting are summarized in figures 3 and 4: figure 3 shows the magnetic excitation energies and figure 4 the relative scattering intensities.

It is clear (figure 2(*a*)) that magnetic excitations of low energy are difficult to resolve from the central coherent peak with the present set-up. In addition, at lower energies there may be several overlapping peaks contributing to the scattering cross section. In order to treat the data in such cases it was necessary to make assumptions about the relative widths of the contributing peaks: the widths were taken to be equal to each other, and to have the same value as that of the peak which was closest in Q but still fully resolved. Nevertheless, the remaining independent parameters in the fit were highly correlated such that low values of $\chi^2(1 \rightarrow 1.3)$ could be obtained for a wide range of combinations of parameters.

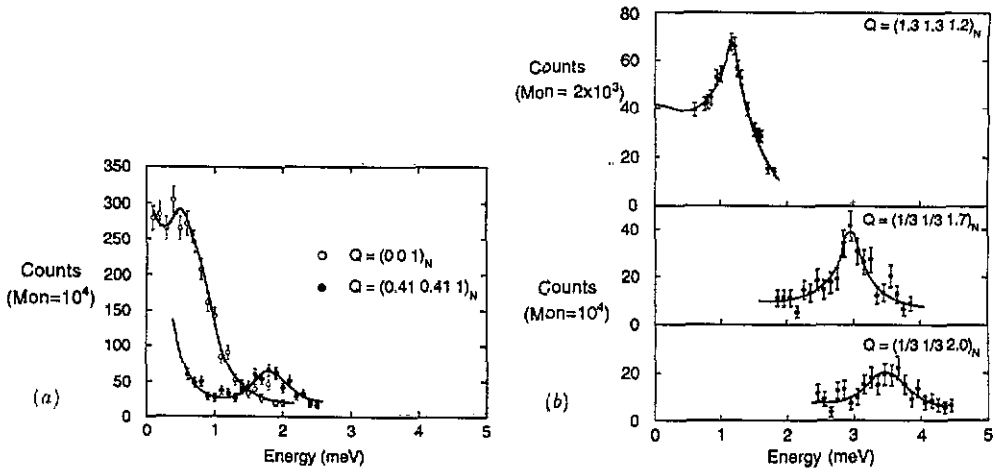

Figure 2. Examples of constant-Q scans on $RbFeBr_3$ at 4.5 K. The value of Q is indicated on the figure, as is the monitor count of the instrument. The full line is the least-squares fit to the data of a scattering background plus a Lorentzian peak convoluted with the instrumental resolution function. (*a*) shows the excitations at $(0\ 0\ 1)_N$ and $(0.41\ 0.41\ 1)_N$, and (*b*) the excitations at $(\frac{1}{3}\frac{1}{3}1.2)_N$, $(\frac{1}{3}\frac{1}{3}1.7)_N$ and $(\frac{1}{3}\frac{1}{3}2)_N$ as indicated on the figure.

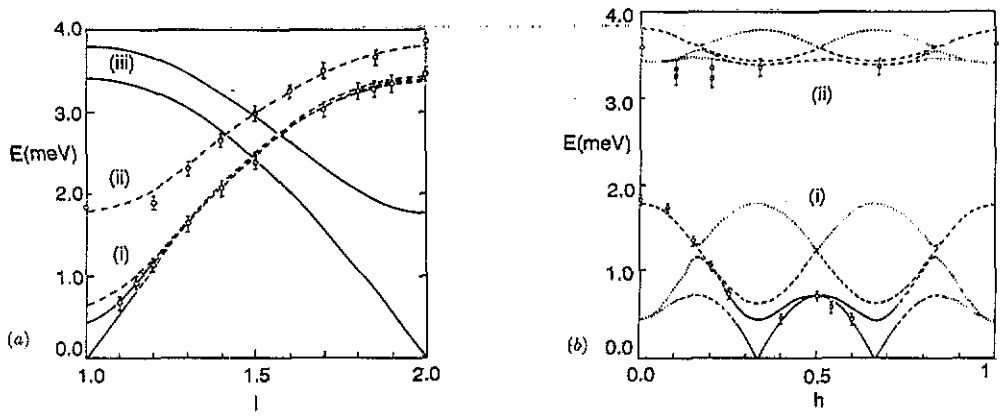

Figure 3. The best fits of the appropriate DCEFA magnon dispersion curves to the data. (*a*) shows the magnon dispersion along (i) $[00l]_N$ and (ii) $[\frac{1}{3}\frac{1}{3}l]_N$ $(l = 1 \rightarrow 2)$ and (*b*) shows the dispersion within the a–b plane in (i) the $[hk1]_N$ direction and (ii) the $[hk2]_N$ direction $(h = k = 0 \rightarrow 1.0)$. In both cases the density of the lines represents the relative magnitude of the calculated scattering cross section. In (*a*) the continuous lines (iii) depict the so-called 'mirror modes' discussed in the text; their scattering intensity is very small.

At higher temperatures the scattering intensities fell off rapidly and limited measurements to low values of Q. The dependence on temperature of energy and scattering intensity of the magnetic excitation peaks at $(0\ 0\ 1)_N$ and $(\frac{1}{3}\frac{1}{3}1)_N$ is displayed in figure 5. The magnetic excitation at $(001)_N$ was a weak scatterer but easily distinguished from the rest of the neutron scattering at this position; the peak at $(\frac{1}{3}\frac{1}{3}1)_N$ appeared as a broad, weak shoulder on the strong central incoherent contribution.

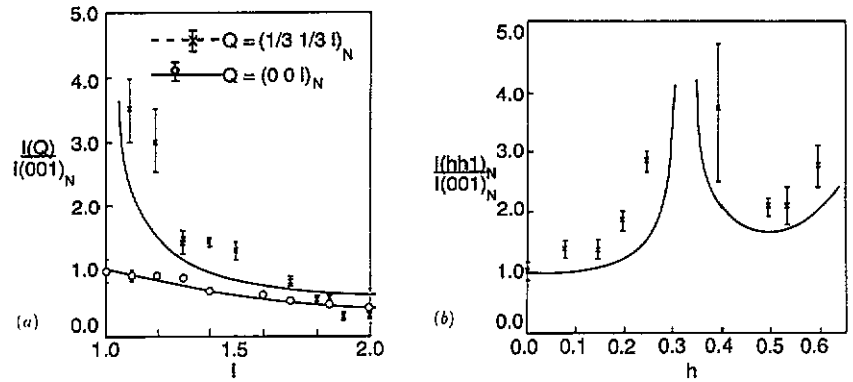

Figure 4. The dependence on wavevector of the inelastic magnetic neutron scattering cross section for the strongest branches observed in our experiments at (*a*) $(\frac{1}{3}\frac{1}{3}l)_N$ and $(00l)_N$ $(l = 1 \rightarrow 2)$ and (*b*) $(hh1)_N$ $(h = 0.0 \rightarrow 0.6)$. The full lines are the results of calculations using the DCEFA model, corrected for the magnetic form factor and the scattering geometry; the crosses are the experimental values. Both the calculated and the experimental values have been normalized to the magnon scattering intensity at $Q = (001)_N$.

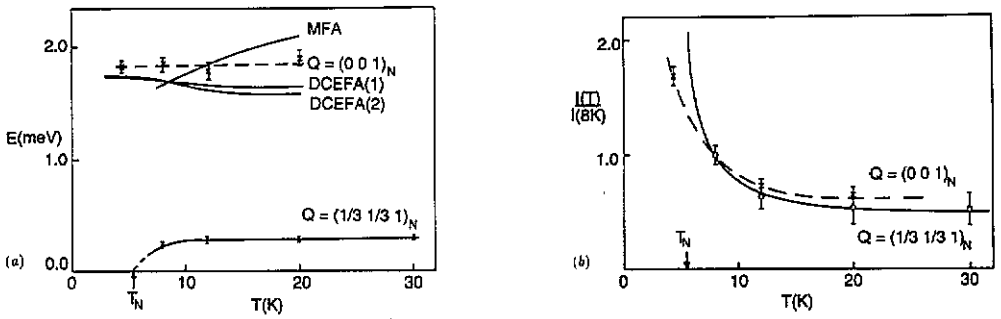

Figure 5. The dependence on temperature of (*a*) the energy and (*b*) the scattering intensity associated with the magnetic excitations at $(001)_N$ and $(\frac{1}{3}\frac{1}{3}1)_N$. In (*a*) the data taken at $Q = (001)_N$ are compared with the results of calculations using the MFA and DCEFA models. In (*b*) the two positions are denoted by dotted and full lines respectively, and the intensities have been normalized to the value at 8 K. The lines are merely a guide to the eye.

5. Analysis and discussion

Initially, estimates were made for the starting values of J_1^γ, J_2^γ and D and the magnetic excitation energies and scattering intensities calculated for all branches. The data points were assigned to particular branches or combinations of branches. The values of J_1^γ, J_2^γ and D were then refined by least-squares fitting these branches to the data.

Dispersion curves have previously been calculated at $T = 0$ and at finite temperatures using an excitonic model with the MFA (Harrison and Visser 1989a): α was set to zero and the self-consistency equation for the ordered moment, $\langle S_\zeta \rangle$, solved numerically. The results of all these fits are presented in table 2. An estimate for T_N was derived from equation (A13) with α and $\omega_i(q)$ set to zero and q set to the magnetic ordering vector $K = (\frac{1}{3}\frac{1}{3}1)_N$.

Table 2. Magnetic exchange parameters (J_i^γ), single-ion anisotropies (D) and correlation parameters (α) for $RbFeCl_3$ and $RbFeBr_3$ derived from inelastic neutron scattering data. The parameters for $RbFeCl_3$ were calculated by Suzuki (1983c) from the data of Petitgrand *et al* (1981). The parameters for $RbFeBr_3$ have been calculated using the DCEFA model and the molecular field approximation (MFA). The three types of DCEFA calculations used were: (1) all parameters taken to be independent; (2) $J_1^\perp/J_1^\parallel = J_2^\perp/J_2^\parallel = \delta$; (3) $J_1^\perp/J_1^\parallel = J_2^\perp/J_2^\parallel = 0.67$ as suggested by Lines and Eibschutz (1975). The effective anisotropy E is defined in equation (A2) of the appendix and J_K is the exchange field in meV experienced by a moment in the magnetically ordered ground state. T_N is the magnetic ordering temperature in K calculated with each model.

	Compound				
Model	$RbFeCl_3$ DCEFA	$RbFeBr_3$ DCEFA(1)	$RbFeBr_3$ DCEFA(2)	$RbFeBr_3$ DCEFA(3)	$RbFeBr_3$ MFA
$J_1^\perp$	0.405	−0.398(10)	−0.400(40)	−0.400(59)	−0.288(4)
$J_2^\perp$	−0.0344	−0.044(3)	−0.044(5)	−0.044(3)	−0.031(5)
$J_1^\parallel$	0.527	−0.431(44)	−0.555(17)	−0.600(88)	—
$J_2^\parallel$	−0.045	−0.065(13)	−0.061(28)	−0.066(46)	—
D	1.92	1.94(2)	2.02(10)	2.07(15)	2.55(4)
E	1.79	1.86	1.85	1.85	
δ	0.77	0.92 0.67	0.72	0.67	
α	0.78	−0.414	−0.418		
J_K	0.91	0.928(30	0.933	0.932	
T_N		2.1	2.15	2.2	6.7

Suzuki (1981, 1983a) asserted that the parameters $J_1^\perp$, $J_2^\perp$, $J_1^\parallel$, $J_2^\parallel$ and D are not independent of each other. He argued that the ratios $J_1^\perp/J_1^\parallel$ and $J_2^\perp/J_2^\parallel$ should be equal and determined by the ratio Δ'/λ'. This is because in the fictitious $S = 1$ Hamiltonian the exchange constants incorporate the orbital contribution to the angular momentum. This assertion is valid if the superexchange pathways along and between the chains make the same use of the σ-bonding 3d orbitals on the iron atoms. It is not valid if there is an appreciable direct component of intrachain exchange arising from overlap of the t_2 orbitals, or any other reason for differing contributions being made by the t_2 and e orbitals to inter- and intrachain exchange.

In our fits of the DCEFA model to the data we first assumed all the parameters in the single-ion Hamiltonian to be independent. We call this procedure DCEFA(1). As a starting point for the fits we assumed the direct contribution to J_1^γ to be negligible. Lines and Eibschutz (1975) used the same assumption to calculate the ratio $J_1^\perp/J_1^\parallel$ to be 1.5. The value of this ratio for $RbFeCl_3$ was calculated by Eibschutz *et al* (1975) to be 1.3, which does not agree well with the value of 0.77 derived by Suzuki (1983c) from inelastic neutron scattering measurements of the magnetic excitations. We have also derived values for J_1^γ and J_2^γ and D subject to the restriction that $J_1^\perp/J_1^\parallel = J_2^\perp/J_2^\parallel = \delta$. This ratio may be allowed to vary or it may be fixed at the value of 1.5 calculated by Lines and Eibschutz (1975). These procedures are called DCEFA(2) and DCEFA(3) respectively. The results of all fits have been listed in table 2. The DCEFA(1) model, with more independent variables, provides a better least-squares fit to the data than the other DCEFA models, but only by about 1%. δ for DCEFA(2) settles at 0.72, which is quite different from the value

provided by Lines and Eibschutz (1975) which was used in DCEFA(3). However, δ and D are highly correlated in the fitting process and consequently the uncertainty in both is high. Thus, without a reliable, independent way of fixing relations between some of the parameters fitted it would be meaningless to try to interpret small differences in the calculated exchange parameters in terms of the magnetostructural trends in these compounds. However, there do seem to be some significant differences in the parameters calculated for $RbFeBr_3$ and $RbFeCl_3$.

(i) The value of J_2' is greater for the bromide than for the chloride. The bridging angle for the two compounds is very similar and the halogen–halogen bond length is also similar, but the larger valence orbitals on the bromine atom are expected to have a larger degree of overlap with the iron atoms. A similar relation is found for the caesium salts (Visser and Harrison 1988).

(ii) The value of D appears to be similar in the two compounds. On the grounds of the structural trigonal distortion away from perfect octahedral symmetry ($\theta = 70.53°$), the bromide with bridging angle $\theta = 72.45°$ should have a smaller value of D than the chloride with $\theta = 73.43°$. This would be reinforced by the greater orbital reduction factor of the bromide (Lines and Eibschutz 1975), which reduces the value of D in the effective $S = 1$ Hamiltonian.

Lindgård (1983) pointed out that the dispersion of magnetic excitations in $CsFeCl_3$ was best described with an expression that included next-nearest-neighbour antiferromagnetic intrachain exchange. He calculated this to be significant relative to J_1 (-0.044 meV compared with 0.262 meV). The effect of this extra term on the predicted magnon dispersion curves is to lower the energy of the lowest branch at $l = 0.5$ relative to that at $l = 1$. An inspection of the appearance of Suzuki's fits of the DCEFA model to inelastic neutron scattering data (Suzuki 1983c) suggests that his model could also be improved in this manner. However, it is less easy to determine the importance of this term in a one-dimensional antiferromagnet because the relative energy of magnons at $(hk0.5)_N$ and $(hk1)_N$ also depends on the balance between D and J_1.

A further test of the ability of the DCEFA model to explain the experimental observations was provided by comparing the calculated and measured scattering intensities. The calculated scattering intensity at a wavevector Q is proportional to the imaginary part of the susceptibility for each branch, as described by Suzuki (1983c). The constant of proportionality contains two Q-dependent factors: one is the geometric factor, $(1 \pm (Q_z/Q)^2)$, and the other is the magnetic form factor for Fe^{2+} (Watson and Freeman 1961). Figure 4 shows the agreement between calculated and measured intensity to be good, though not significantly different from the results of the MFA fits reported by Harrison and Visser (1989a).

The DCEFA model is less successful at predicting the behaviour of $RbFeBr_3$ at or near T_N. Using the optimized values of the exchange parameters obtained from the fits to the magnon dispersion curves, a value of 2.1 ± 0.1 K was deduced for T_N using equation (A13) from the appendix with the value of α calculated self-consistently with expression (A17). The temperature dependence of the energy of the magnetic excitation at $(001)_N$ was successfully predicted (figure 5), but not that at the H point ($Q = (\frac{1}{3}\frac{1}{3}1)_N$ (figure 6). The failure to predict T_N correctly may be largely due to the way in which the DCEFA model has been implemented. We used an expression appropriate for $T = 0$ to obtain exchange parameters from data taken at about $T = 0.8T_N$. At this temperature the effective exchange paramcters may

be significantly smaller than those at $T = 0$ and the predicted value of T_N would consequently be lower. The MFA method is more successful at predicting T_N, giving a value of $T_N \simeq 6.7$ K. However, when the temperature dependence of the energy of the magnetic excitation at the A point ($Q = (001)_N$ is calculated using the DCEFA models and the MFA models; the DCEFA(1) model is found to give the best treatment of the data (figure 5(*a*)). Furthermore, the DCEFA models (1) and (2), in which the ratio $J_1^{\perp}/J_1^{\parallel}$ is appreciably smaller than that calculated by Lines and Eibschutz (1975), are also significantly better at treating the temperature dependence of the energy of the same magnetic excitation. This suggests that $J^{\parallel}$ is anomalously high relative to $J^{\perp}$. One explanation for this is that there *is* a significant direct component of magnetic exchange in $RbFeBr_3$ and $RbFeCl_3$. However, this implies that the direct exchange is ferromagnetic for $RbFeCl_3$ and antiferromagnetic for $RbFeBr_3$, which is unlikely because the orbitals that would be involved in such coupling should be of the same symmetry in both compounds. Consequently the direct exchange should have the same sign in both cases.

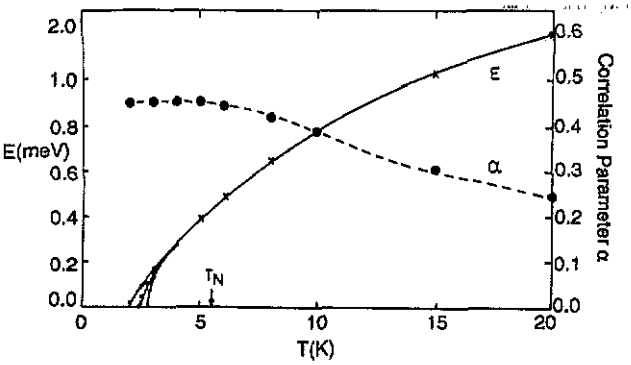

Figure 6. The dependence on temperature of the energy of the magnon at $(\frac{1}{3}\frac{1}{3}1)_N$ as calculated by the DCEFA model. This is represented by the full lines through the crosses. The calculated value of T_N is seen to increase as the fineness of the grid used in the numerical integration in equation (A17) increases. The full circles represent the values of the correlation parameter α. The values of J_1', J_2' and D used in the calculations are the ones given in table 2.

The reason for the discrepancy between the theoretical and experimental value of the energy of the magnetic excitation at the H point probably lies in the experimental data. On comparison with the renormalization of the energy of the magnetic excitation at the K point in $RbFeCl_3$ and $CsFeCl_3$ (Yoshizawa *et al* 1980), our data appear anomalous. The strength of the coherent scattering intensity at the H point obscures the inelastic excitations with low cross section. A fuller experimental study using an instrument of higher resolution is needed to settle this issue.

The present set of data do not provide firm evidence for a magnetically ordered phase below T_N other than the regular triangular structure. Even if such a phase did exist at 4.5 K it is very unlikely that the difference between J_2(A–B) and J_2(B–B) would be sufficient to produce a splitting in the energy of the magnetic excitations at $(0\ 0\ 1)_N$ and $(\frac{1}{2}\frac{1}{2}1)_N$ that could be resolved with Pluto TAS. However, a set of measurements of the magnetic excitations at these points over a range of temperatures might reveal a change in the width in energy of the excitations. Certainly the

excitation at $(0\ 0\ 1)_N$ was broader than those at $(0.08\ 0.08\ 1)_N$ and at $(0.15\ 0.15\ 1)_N$, with resolution-corrected energy widths of 0.60(13), 0.39(10) and 0.40(10) meV respectively. Further measurements are needed to show that these values are reliable.

In the present study the magnetic excitations in $RbFeBr_3$ have been presented in the extended zone scheme. In addition to the distinct excitations observed at $[\frac{1}{3}\frac{1}{3}l]_N$ and $[00l]_N$ for $l = 1 \rightarrow 2$, which correspond to in-plane (xy) fluctuations, we expect a second set of excitations corresponding to the out-of-plane (zz) fluctuations. The latter set are obtained from the former by folding the dispersion curves about $l = 1.5$. The scattering cross sections of the second set of excitations are, however, very weak. An example of the scattering strengths of these 'mirror modes' relative to the modes that we observed is given in figure 7. In the case of the excitations along $[00l]_N$ the scattering cross section is reduced to zero by the geometric factor $(1 \pm (Q_z)/Q)^2)$. In our measurements no such branches were seen. It was claimed that such branches could be seen in the isomorphous singlet ground state antiferromagnet $CsFeBr_3$ (Visser and Steigenberger 1984, Dorner *et al* 1988) but more recent measurements using neutron polarization analysis and the temperature dependence of the inelastic neutron scattering demonstrated that the 'mirror modes' observed to date are artefacts (Visser *et al* 1991b, Schmid *et al* 1992a).

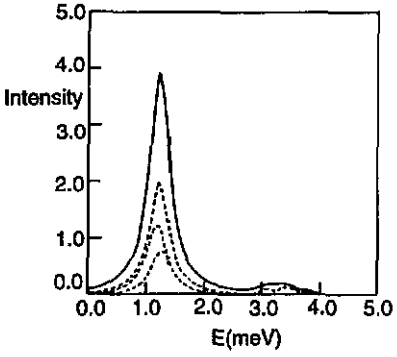

Figure 7. A simulation of an inelastic neutron scattering constant-Q scan at $Q = (\frac{1}{3}\frac{1}{3}1.2)_N$. The energy and scattering cross section of each magnon at this wavevector was calculated using the DCEFA model, corrected for the magnetic form factor and the geometric term $1 \pm (Q_z/Q)^2$ and convoluted with the instrumental resolution function. The units of intensity are arbitrary. This demonstrates the weakness of the scattering from the 'mirror modes'.

6. Conclusions

Suzuki's DCEFA model is successful in explaining the form of the inelastic magnetic neutron scattering from $RbFeBr_3$ below the magnetic ordering temperature: the energies and scattering intensities of the magnetic excitations are treated well, and the optimized values of J_1, J_2 and D relate in a sensible way to the values derived for $RbFeCl_3$ in the same manner. There is less success in predicting the value of T_N from the values of these parameters. Further experiments are needed to test the predictions of Suzuki and Shirai (1986), measuring the magnetic excitation dispersion within the a–b plane with greater resolution, over a range of temperatures.

A comparison between the DCEFA and MFA models is inconclusive, and suggests that further measurements are needed, using a variety of experimental probes over a wider range of temperatures. However, discrepancies in both models might arise through the neglect of magnon–magnon interactions. An adequate treatment of this effect requires a fuller correlation theory such as that of Lindgård (1984b).

Acknowledgments

The authors wish to express their thanks to Dr N Suzuki of Osaka University for his invaluable help with the DCEFA calculations, for stimulating discussions and the loan of his computer programs. Thanks are also due to Dr P J Walker of the Clarendon Laboratory, Oxford for growing the sample of $RbFeBr_3$. We thank Mr N Clarke and Mr P Bowen at AERE, Harwell for their technical assistance with the experiment. We are grateful to SERC for financial support and to Dr P Day of this laboratory for his encouragement and provision of research facilities. AH is grateful to St John's College, Oxford and to the Royal Society for financial support.

Appendix

We derive an expression for the determination of α in the paramagnetic phase. First we establish Suzuki's DCEFA model. The coordinate system used involves the rotating coordinates (ξ, η, ζ) in which η is parallel to the crystal c-axis, ζ parallel to the equilibrium spin direction at each site and ξ perpendicular to both these axes. The effective single-ion Hamiltonian is then

$$H_i^{\text{eff}} = ES_{i\eta}^2 - BS_{i\zeta} \tag{A1}$$

where

$$E = D + \alpha(J_0^{\perp} - J_0^{\parallel}) \tag{A2}$$

and

$$B = 2(J_K^{\perp} - \alpha J_0^{\perp})\langle S_\zeta \rangle. \tag{A3}$$

J_q is the Fourier transform of the exchange integral:

$$J_q = 2J_1 \cos(2\pi q_c) + 2J_2\{\cos(2\pi q_a) + \cos(2\pi q_b) + \cos(2\pi(q_a + q_b))\} \tag{A4}$$

where J_K is the value of J_q when q equals the helical magnetic ordering vector K. $\langle S_\zeta \rangle$ is determined self-consistently from

$$\langle S_\zeta \rangle = \sum_i \langle i|S_\zeta|i\rangle \rho_i \tag{A5}$$

$$= 2B(\rho_0 - \rho_2)/W \tag{A6}$$

where ρ_i is the Boltzmann population of the S_i levels $i = 0, 1, 2$ and the correlation parameter α is calculated in the fashion described by Suzuki (1983b, c) using the expression:

$$\langle\{S_{i\xi},\ S_{j\xi}\}\rangle = (1/N)\sum_{q}(1/\pi)\int d\omega \coth((\beta\omega)/2)\mathrm{Im}\,\chi^{\xi\xi}(q,\omega). \tag{A7}$$

The left-hand side of this equation simplifies:

$$\langle\{S_{i\xi},\ S_{j\xi}\}\rangle = \langle S_i^+ S_j^- + S_i^- S_j^+\rangle \tag{A8}$$

$$= 1 + \rho_1 + E(\rho_0 - \rho_2)/W. \tag{A9}$$

In the paramagnetic state $\langle S_\zeta\rangle$ is set to zero and $\chi^{\xi\xi}(q,\ \omega)$ then becomes $\chi^{\perp}(q,\ \omega)$, given by

$$\chi^{\perp}(q,\omega) = \phi^{\perp}(\omega)/[1 - (J_q^{\perp} - \alpha J_0^{\perp})\phi^{\perp}(\omega)] \tag{A10}$$

where

$$\phi^{\perp}(\omega) = -4E\rho/(\omega^2 - E^2) \tag{A11}$$

and

$$\rho = (e^{\beta E} - 1)/(e^{\beta E} + 2). \tag{A12}$$

$\chi^{\perp}(q,\omega)$ has poles at energies $\omega_i(q)$ given by

$$\omega_i^2(q) = E^2 - 4E\rho(J^{\perp}q - \alpha J_0^{\perp}). \tag{A13}$$

Therefore

$$\chi^{\perp}(q,\omega) = -4E\rho/(\omega^2 - (\omega_i^2 q)) \tag{A14}$$

$$= \frac{-2E\rho}{\omega_i(q)}\left(\frac{1}{\omega - \omega_i(q)} - \frac{1}{\omega + \omega_i(q)}\right). \tag{A15}$$

Using the identity

$$\lim_{\mathrm{Lim}\epsilon\to 0}\mathrm{Im}\left(\frac{1}{(\omega - \omega_i(q) - i\epsilon)} - \frac{1}{(\omega - \omega_i(q) + i\epsilon)}\right) = 2\pi\delta(\omega - \omega_i(q)). \tag{A16}$$

We find that (A9) becomes

$$1 + \rho_0 = 4E\rho\sum_{q}\coth((\beta\omega)/2) + (1/\omega_i(q)). \tag{A17}$$

References

Achiwa N 1969 *J. Phys. Soc. Japan* 27 561
Adachi K, Takeda K, Matsubara F, Mekata M and Haseda T 1983 *J. Phys. Soc. Japan* 52 2202

Baines J A, Johnson C A and Thomas M F 1983 *J. Phys. C: Solid State Phys.* **16** 3579
Buyers W J L, Holden T M and Perreault A 1975 *Phys. Rev.* B **11** 266
Callen H B 1963 *Phys. Rev.* **130** 890
Chiba M, Ajiro Y, Adachi K and Morimoto T 1988 *J. Phys. Soc. Japan* **57** 3178
Dickson D P E 1981 cited in Baines *et al* (1983)
Dorner B, Visser D, Steigenberger U, Kakurai K and Steiner M 1988 *Z. Phys.* **72** 487
Dorner B, Visser D and Steiner M 1990 *Z. Phys.* B **81** 75
Eibschutz M, Lines M E and Sherwood R C 1975 *Phys. Rev.* B **11** 4595
Goodenough J B 1960 *Phys. Rev.* **100** 564
Harrison A 1986 *D Phil Thesis* Oxford University
Harrison A, Stager C V and Visser D 1991 *J. Appl. Phys.* **69** 5998
Harrison A and Visser D 1989a *Phys. Lett.* **137A** 79
—— 1989b *J. Phys.: Condens. Matter* **1** 733
Haseda T, Wada N, Hata M and Amaya K 1981 *Physica* B **108** 841
Hatfield W E, Estes W E, Marsh W E, Pickens M W, ter Haar L W and Weller R R 1983 *Extended Linear Chain Compounds* vol 3, ed J S Miller (New York: Plenum)
Knop W and Steiner 1984 private communication
Knop W, Steiner M and Day P 1983 *J. Magn. Magn. Mater.* **31–4** 1033
Lindgård P A 1983 *Physica* B **120** 190
—— 1984a *Condensed Matter Research Using Neutrons (NATO ASI Series B 112)* ed S W Lovesey and R Scherm (New York: Plenum) p 163
—— 1984b *Phys. Rev.* B **30** 2729
Lines M E 1974 *Phys. Rev.* B **9** 3927
Lines M E and Eibschutz M 1975 *Phys. Rev.* B **11** 4583
Loveluck J M and Lovesey S W 1975 *J. Phys. C: Solid State Phys.* **8** 3857
Montano P A, Cohen E, Shechter H and Makovsky J 1973 *Phys. Rev.* B **7** 1180
Montano P A, Shechter H, Cohen E and Makovsky J 1974 *Phys. Rev.* B **9** 1066
Plumer M L and Caillé A 1991 *J. Appl. Phys.* **70** 5961
Putnik C F, Cole G M, Garrett B B and Holt S L 1976 *Inorg. Chem.* **15** 189
Schmid B, Dorner B, Visser D and Steiner M 1992a *Z. Phys.* B **86** 257
—— 1992b *J. Magn. Magn. Mater., Proc. 1991 Int. Conf. on Magnetism* **104–107** 771
Shiba H and Suzuki N 1982 *J. Phys. Soc. Japan* **51** 3488
Steiner M, Kakurai K, Knop W, Dorner B, Pynn R, Happek Y, Day P and McLeen G 1981 *Solid State Commun.* **38** 1179
Suzuki N 1981 *J. Phys. Soc. Japan* **50** 2931
—— 1983a *J. Phys. Soc. Japan* **52** 1002
—— 1983b *J. Phys. Soc. Japan* **52** 1009
—— 1983c *J. Phys. Soc. Japan* **52** 3907
Suzuki N, Isu T and Motizuki K 1977 *Solid State Commun.* **23** 319
Suzuki N and Shirai M 1986 *Physica* B **136** 346
Visser D 1990 Private communication
Visser D, Dorner B and Steiner M 1991a *Physica* B **174** 25
—— 1991b *Z. Phys.* B submitted
Visser D and Harrison A 1988 *J. Physique Coll.* **C8** 1467
Visser D and Prodan A 1980 *Phys. Status Solidi* **A58** 481
Visser D and Steigenberger U 1984 *Annex to the Annual Report of the Institut Laue–Langevin* p 92
Wada M, Ubokoshi K and Hirakawa K 1982 *J. Phys. Soc. Japan* **51** 283
Watson R E and Freeman A J 1961 *Acta Crystallogr.* **14** 27
Yoshizawa H, Kozukue W and Hirakawa K 1980 *J. Phys. Soc. Japan* **49** 144